Proceedings of the ASME 2024
International Design Engineering Technical Conferences and
Computers and Information in Engineering Conference
IDETC/CIE 2024
August 25-28, 2024, Washington, DC

IDETC2024-142038

A NOVEL CONNECTIVITY INDEX FOR MICROSTRUCTURES IMPERFECTION DETECTION AND RECTIFICATION IN MULTISCALE STRUCTURE DESIGN

Sina Rastegarzadeh, Jida Huang*

Department of Mechanical and Industrial Engineering, University of Illinois Chicago, Chicago, Illinois 60607

ABSTRACT

Inspired by natural designs, microstructures exhibit remarkable properties, which drive interest in creating metamaterials with extraordinary traits. However, imperfections within microstructures and poor connectivity at the microscale level can significantly impact their performance and reliability. Achieving proper connectivity between microstructural elements and detecting structural imperfections within the microstructures pose challenges in multiscale design optimization. While using a connectivity index (CI) to quantify the topological connectivity between microstructures has been explored previously, prior approaches have limitations in identifying microstructures with complex curved geometries between adjacent units. To alleviate this issue, we present a novel CI in this study. The proposed CI goes beyond conventional methods by focusing on surface interfaces and internal microstructural irregularities. Through numerical investigations, we successfully connected distinct types of microstructures well by integrating the introduced CI with the functional-gradation scheme. We also demonstrate that the presented CI can serve as a metric to identify sharp changes or imperfections within microstructures. We evaluate the performance of the introduced index against other connectivity indices using diverse microstructural examples. Experimental findings provide valuable insights into the fundamental aspects of imperfection detection and rectification in microstructures within the multiscale design, paving the way for developing more robust and reliable materials in engineering applications.

1. INTRODUCTION

In nature, an abundance of materials and structures showcase intricately designed microstructures that possess exceptional properties. For instance, the nacre exhibits high stiffness and toughness [1], bamboo possesses impressive bending stiffness [2], and deep-sea glass sponges feature remarkable porosity [3]. Moreover, there is a burgeoning interest in engineering various microstructural attributes observed in nature [4, 5] and creating metamaterials with extraordinary properties rarely found in natural [6–8]. Thanks to recent advances in additive manufacturing technology, the fabrication of geometrically complex microstructures has become increasingly feasible.

Many studies have delved into crafting microstructures to tailor the properties of engineered materials [9, 10]. Advancing this pursuit, multi-scale topology optimization (TO) techniques have emerged, which enables the concurrent design of both macroscopic structures and their corresponding microstructures [11–13]. For instance, Zhu et al. [14] introduced a novel computational framework for topology optimization with microstructures, accommodating design spaces of multiple dimensions. Chen et al. [15] outlined a two-scale topology optimization methodology employing the moving iso-surface threshold (MIST) method, aimed at simultaneous design of structures and their material microstructures. Meanwhile, Sanders et al. [16] pioneered the integration of design and manufacturing processes for spatially diverse hierarchical structures using a multimicrostructure topology optimization framework. Despite progress, these methods are constrained by a set of predefined non-periodic transitional unit cells, posing challenges in characterizing homogenized mechanical properties [17]. Attempts have been made to address the aforementioned challenges through the use of functional representation (FRep) of architected materials. Extending the classical multi-scale homogenization-based topology optimization proposed by Bendsoe and Kikuchi [18], Senhora et al., [4] formulated a multi-scale design approach accommodating multiple candidates of spinodal cellular structures, optimizing their locally-varying microscale orientation and density.

In most multi-scale optimization approaches, the asymptotic homogenization theory [18] has been commonly employed to derive the effective material properties of periodic microstructures. However, this method tends to overlook the connectivity between adjacent microstructures [12, 19, 20]. As shown in (Fig. 1), poor connectivity between adjacent microstructures can impair manufacturability and lead to load transition issues at the macro-level,

*Corresponding author: jida@uic.edu

Copyright © 2025 by ASME

thus deviating significantly from the approximated effective homogenized behavior [21].

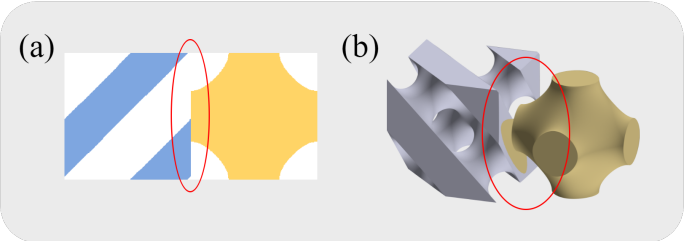

FIGURE 1: IMPROPER CONNECTIVITY BETWEEN ADJACENT MICROSTRUCTURES: (A) THE POOR CONNECTIVITY BETWEEN TWO 2D MICROSTRUCTURES, AS HIGHLIGHTED IN THE OVAL AND (B) THE POOR CONNECTIVITY BETWEEN TWO 3D MICROSTRUCTURES, AS HIGHLIGHTED IN THE OVAL.

To address the connectivity issue, Alexandersen and Lazarov [22] proposed directly optimizing microstructures using an extremely fine mesh to ensure connectivity. However, despite efforts to minimize computational costs, this method remains notably more resource-intensive than homogenization-based approaches. Addressing boundary layer stresses differently, Xie et al. [23] introduced new micro-stresses as the sum of the microscopic stresses of classical homogenization and boundary layer stresses. Results from similar studies [23–25] indicate that the homogenization method can effectively provide a reasonable approximation for a significant number of repeated unit cells, especially when considering certain global measures such as mean compliance. Yet the real challenge is to ensure smooth microstructural connectivity without compromising mechanical behavior accuracy [26].

To alleviate the computational issue, several studies [21, 27–30] have investigated the connectivity issue without introducing extra computational cost. A metric is proposed to explicitly measure the connectivity between unit cells and integrate it into the TO framework. Specifically, a connectivity index (CI) is designed to quantify the topological connectivity between two neighboring microstructures, which later acts as a constraint in the multi-scale topology optimization process. CI is a normalized connectivity index between o and 1, $CI = 1$ means no connection (Fig. 2a), and $CI = 0$ means a perfect connection between two adjacent microstructures (Fig. 2b). Although the introduced CI approach proves highly effective in the majority of cases, previously introduced CI metric[21] can falsely indicate a poor connection ($0 << CI < 1$) case, though microstructures are perfectly connected to each other (see Fig. 2c,d).

To address the incapability of CI and improve its effectiveness, this paper presents a novel Connectivity Index (CI) designed to measure and quantify the connections between microstructures accurately. The proposed metric can effectively identify the imperfections within the unit cells in multi-scale design problems and is compatible with various optimization algorithms. Moreover, a connectivity-enhancing scheme is induced based on the proposed CI. Thus, the proposed CI not only identifies the poor connectivity but also serves as a foundation for improving the imperfections between adjacent microstructures. To demonstrate the validness and effectiveness of the proposed approach, several

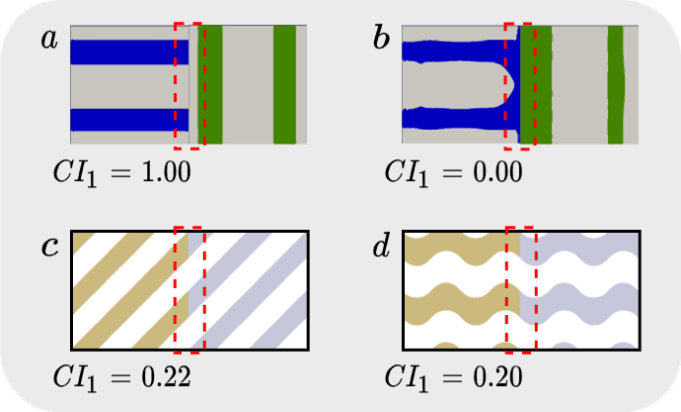

FIGURE 2: CHALLENGES SEEN IN THE EXISTING METHODS TO QUANTIFY THE CONNECTIVITY OF MICROSTRUCTURES. THE CI_1 VALUES ARE CALCULATED USING THE FORMULA PROVIDED IN [21]. A $CI_1 = 1$ INDICATES AN ISOLATION AND A $CI_1 = 0$ INDICATES A PERFECT CONNECTION BETWEEN TWO ADJACENT MICROSTRUCTURE. A) A CASE WITH COMPLETE DISCONNECTION [21], B) A MODIFIED CONNECTION [21], C) AN EXAMPLE OF A PERFECT CONNECTION WITH $CI_1 = 0.22$ WHICH IS AN INDICATOR OF A BAD CONNECTION. D) AN EXAMPLE OF A PERFECT CONNECTION WITH $CI_1 = 0.20$ WHICH INDICATES A BAD CONNECTION.

examples of the common functionally grading microstructures [16, 31] and triply periodic minimal surfaces (TPMS)-based microstructures are employed. Both 2D and 3D microstructures are studied and compared to the previously introduced connectivity index metric [21]. Experimental results reveal that our proposed work can identify poor connectivity cases while the previous work [21] cannot, and a naturally enhancing scheme induced by the proposed CI is conducted to address the imperfections. To this end, the key contributions of our work can be summarized as follows:

- Introduced of a novel Connectivity Index (CI) that overcomes the limitations of previously introduced metrics.
- Exploited the introduced CI to devise an imperfection-enhancing scheme to achieve seamless transitions between distinct types of microstructures without requiring specialized post-processing treatment.
- Verified the validness and effedtines of the introduced CI in identifying imperfections within the unit cells and the CI-induced imperfection-enhancing scheme.

The remainder of the paper is organized as follows. In Section 2, a new explicit CI is proposed to measure the connectivity of microstructures in multi-scale design problems. The introduced CI is applied to functionally represented microstructures in Section 3, followed by some concluding remarks in Section 4.

2. CONNECTIVITY OF MULTI-SCALE DESIGN

2.1 Connectivity Index

Having a metric to quantify the connectivity between microstructures makes it more efficient to address the connectivity

Copyright © 2025 by ASME

challenges in multi-scale design frameworks. There are different ways to address the connectivity issue [4, 16, 31–33]. A connectivity index helps us select the best solution and achieve seamless transitions between cellular structures while maintaining desired mechanical properties. This advancement could revolutionize the design and optimization of complex engineered materials with tailored microstructures.

The previously introduced CI_1 [21] is defined using a local interface region of the mutual boundary, see Fig. 3 left column. This CI_1 is a normalized symmetry measure of the material distribution in the interface regions, and it can be defined as:

$$CI_1 \triangleq \frac{\sum_{i=1}^{2} \int_{S_i} H(\Phi_i(p))(1 - H(\Phi_j(Rp)))ds}{\sum_{i=1}^{2} \int_{S_i} H(\Phi_i(p))ds}, \quad i \neq j;\ i, j = 1,\ 2 \tag{1}$$

where S_i is the strip region colored in light red near the adjacent cell of i_{th} microstructure. R denotes the mirror reflection operator, which maps a point $\mathbf{x}$ to its symmetric counterpart R$\mathbf{x}$ in the adjacent cell; H is a Heaviside step function; and Φ_i is the level function of $i_t h$ microstructure.

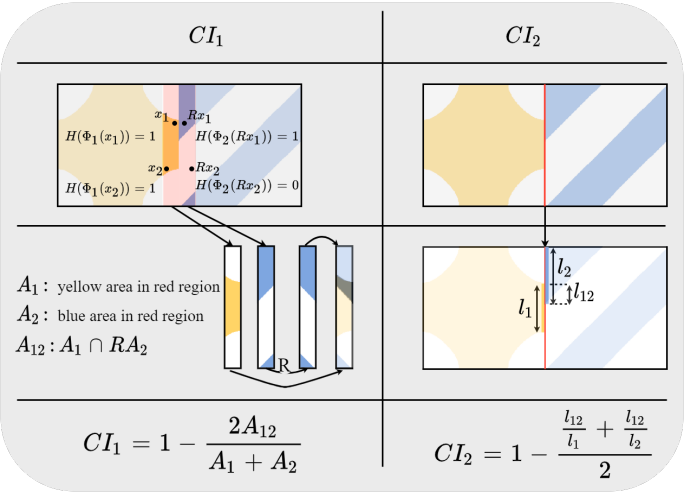

FIGURE 3: AN ILLUSTRATION OF THE PREVIOUSLY INTRODUCED CI_1 [21], AND THE PROPOSED CONNECTIVITY METRIC CI_2. THE YELLOW AND BLUE STRUCTURES REPRESENT TWO ADJACENT UNIT CELLS. CI_1: A_1 IS THE YELLOW AREA IN THE RED STRIP REGION; A_2 IS THE BLUE AREA IN THE RED STRIP REGION; AND A_{12}, IS THE INTERSECTION OF YELLOW IN RED AREA (A_1) AND MIRRORED OF BLUE IN RED AREA (RA_2). CI_2: l_1 IS THE YELLOW LINE; l_2 IS THE BLUE LINE; AND l_{12} IS THE INTERSECTION OF YELLOW AND BLUE LINES.

Based on the CI_1 definition, Two neighboring microstructures are completely disconnected when $CI_1 = 1$ (Fig 2a), and are perfectly connected when $CI_1 = 0$ (Fig 2b), which implies that their connection regions are symmetric about the interface. However, it's important to note that this metric is effective only for connection regions that exhibit symmetry about the interface. There are instances where perfectly connected unit cells lack symmetry about their interface, leading to misclassification by this metric (Fig. 2c ,d).

This misclassification problem can be solved by introducing a new CI independent of the material distribution symmetry. To do that, we have prescribed the width of the strip region infinitesimally small and rewrote the Eq. (1). For a 2D material, the new connectivity index is defined as:

$$CI_2 \triangleq \frac{\sum_{i=1}^{2} \int_{L_i} H(\Phi_i(p))(1 - H(\Phi_j(Rp)))dl}{\sum_{i=1}^{2} \int_{L_i} H(\Phi_i(p))dl}, \quad i \neq j;\ i, j = 1,\ 2 \tag{2}$$

where L_i is the line colored in light red near the adjacent cell of i_{th} microstructure (the strip region for a 2D material will be a line and for a 3D material would be a plane). We will demonstrate that the new CI_2 has no longer the misclassification issued that CI_1 has. In numerical implementation, CI_1 and CI_2 can be calculated as:

$$CI_1 = 1 - \frac{2A_{12}}{A_1 + A_2}, \quad CI_2 = 1 - \frac{\frac{l_{12}}{l_1} + \frac{l_{12}}{l_2}}{2} \tag{3}$$

In CI_1 formula, $A_1 = \int_{S_1} H(\Phi_1(p))ds$ which is the yellow area in the red strip region in Fig. 3; $A_2 = \int_{S_2} H(\Phi_2(p))ds$ which is the blue area in the red strip region in Fig. 3; and $A_{12} = \int_{S_1} H(\Phi_1(p))H(\Phi_2(Rp))ds$, which is the intersection of yellow in red area (A_1) and mirrored of blue in red area (RA_2). While in CI_2 formula, $l_1 = \int_{L_1} H(\Phi_1(p))dl$ which is the yellow line in Fig. 3, CI_2 column; $l_2 = \int_{A_2} H(\Phi_2(p))dl$ which is the blue line in Fig. 3; and $l_{12} = \int_{L_1} H(\Phi_1(p))H(\Phi_2(Rp))dl$, which is the intersection of yellow (l_1) and blue line (l_2). It should be noted that since the considered regions in calculation of CI_2 are lines, we can write $H(\Phi_i(Rp)) = H(\Phi_i(p))$; and that is how we have developed a connectivity index independent of the symmetry of material distribution.

2.2 Design Units

Without losing the generality, we chose implicitly represented cellular materials for the numerical demonstrations. Implicitly represented cellular solids are architected materials that are described by parameterized implicit functions. They can generate cellular solids that possess various material properties. In this work, we have used both 2D and 3D functionally represented cellular materials to design the sample microstructures. The 2D version of these types of microstructures are developed from a level function which can be described by an implicit function as follows:

$$F : \mathbb{R}^2 \rightarrow \mathbb{R} \quad \{(x, y) \in \mathbb{R}^2 | \Phi(x, y) = F(x, y) - t\} \tag{4}$$

where $F(x, y)$ is an implicit function, t is the design parameter. Changing the design parameter t would create distinct members of a given family of level surfaces. The area defined by $\Phi(x, y) > 0$ is the target microstructure. Fig. 4 shows that adjusting parameter t can change the surface area. Hence, it can be used as a design parameter to control the relative density ρ of the microstructure.

To demonstrate the efficacy of the proposed CI metric, we have selected seven implicitly-represented cellular materials for

Copyright © 2025 by ASME

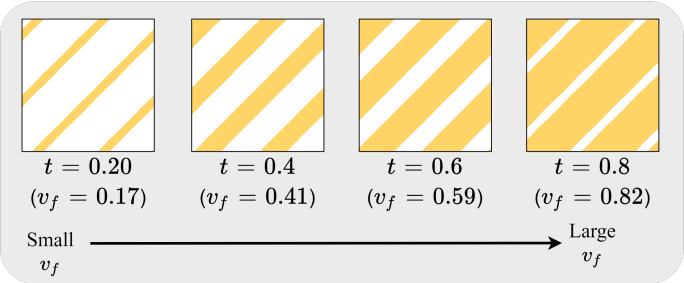

FIGURE 4: ILLUSTRATION OF HOW THE DESIGN PARAMETER t INFLUENCE THE TOPOLOGY OF THE MICROSTRUCTURE AND CONTROL THE RELATIVE DENSITY OF THE MICROSTRUCTURE. THE RELATIVE DENSITY IS DEFINED AS THE RATIO OF THE AREA OF THE YELLOW COLOR REGION TO THE AREA OF THE SQUARE.

analysis. Moreover, the calculation of CI_2 can be extended to any type of cellular structure, as its definition is not dependent on the material under consideration. The seven typical microstructures exploited here include four common TPMS-based cellular materials (gyroid (F_G), diamond (F_D), Primitive (F_P), and I-WP (F_W) [34]) and three Fourier series function (FSF)-based cellular materials. More details of modeling cellular materials using the implicit functions can be found in our previous works [35, 36].

2.3 CI-Induced Imperfection-Enhancing Scheme

With the development of the new CI_2 metric, we can now pinpoint weak connections at the microstructure interfaces with remarkable precision. Any interface exhibiting a significantly large connectivity index ($0 << CI_2 <= 1$), indicates a poor connection. Using this tool, we can now turn our attention to improving these connections and enhancing the structure's robustness. One of the most successful approaches to improving the connection at the micro-level is spatial gradation. This approach generates a functionally graded microstructure by interpolating the two adjacent unit cells. Both weighted interpolation and linear interpolation have been used in developing this approach. We choose the weighted approach where the weights are carefully defined to control the length of the transition area and the sharpness of the transition. These weights are determined as functions of the Euclidean distances to the center of the surrounding microstructures from the developed CI as in Eq. (2).

$$\omega_i = e^{-\kappa \mathbf{d_i}}, \quad i = 1, ..., n \tag{5}$$

here ω is the weight function, κ is the control parameter, $\mathbf{d}$ is the Euclidean distance function, and n is the number of microstructures. The transition region length and the connection interface between the microstructural materials are affected by the κ, the interpolation weight function's parameter.

Figure 5 illustrates how weight functions are calculated for two sample microstructural materials and how they can affect the interface transition length. The ability to tailor weight functions ω_i in microstructure design plays a crucial role in achieving smooth transitions and enhancing load transmission at interface boundaries. While Eq. (5) exemplifies how numerous unique weight functions can be generated via the κ parameter, the question remains as to which specific function yields the most well-connected interface. Previously, determining the optimal κ relied heavily on experimentation. However, utilizing the CI_2 metric, we now have a powerful tool to find the ideal value. By minimizing CI_2 as a function of κ, we can systematically identify the weight function that fosters the most robust and seamless connections.

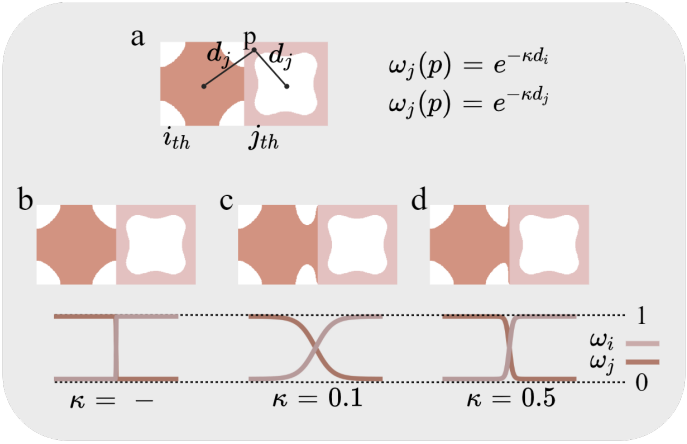

FIGURE 5: ILLUSTRATION OF HOW WEIGHTED INTERPOLATION INFLUENCE THE TRANSITION BETWEEN TWO MICROSTRUCTURE. A) WEIGHTS ARE FUNCTIONS OF EUCLIDEAN DISTANCES TO THE CENTER OF EACH UNIT CELL AND THE CONTROL PARAMETER (κ). VARYING THE κ CHANGES THE SIGMOID CURVE AND STRETCH OR TIGHTEN THE TRANSITION ZONE. B) HOW TWO UNIT CELL ARE CONNECTED TO EACH BEFORE APPLYING THE WEIGHTED INTERPOLATION. C) AN SMALL κ CREATE A LARGER TRANSITION REGION. D) A LARGER κ CREATE A SHORTER TRANSITION REGION.

This integration of CI_2 into the design process empowers engineers and scientists with unprecedented control to optimize the structure for robustness by addressing the connectivity issue. They can now objectively compare and optimize various stochastic microstructure designs, ensuring they align with their specific application requirements and performance goals. This data-driven approach eliminates the need for subjective judgments and guesswork, leading to more efficient and effective design outcomes.

3. NUMERICAL EXPERIMENTAL RESULTS

In this section, we delve into a numerical investigation of the connectivity index function within microstructure optimization by comparing the metrics CI_1 and CI_2. For our validation study, we studied six trivial yet properly connected pairs of microstructures. Additionally, we construct particularly challenging two-cell structures featuring a single interface, where the topologies of the two adjacent cells exhibit poor connectivity. Subsequently, we proceed to optimize the microstructures by minimizing the CI_2 to achieve a proper connection, improving the load transfer, and smooth transition between microstructures.

3.1 Addressing Connectivity Issue with Proposed CI

In this section, we embarked on testing the efficacy of the CI_2 metric through various practical examples to assess its per-

Copyright © 2025 by ASME

formance in quantifying the connection between microstructures. The selection process was deliberate, encompassing six pairs of microstructures, with three exhibiting symmetry about their interface and three lacking such symmetry. This deliberate configuration aimed to offer diverse scenarios for evaluation. The microstructures chosen were known to possess a perfect connection, ensuring a baseline for comparison.

As illustrated in Figure 6, the CI_2 metric demonstrated its effectiveness by yielding values close to zero ($CI_2 \simeq 0$) across all six cases. This close approximation to zero signifies a proper connection, aligning with our expectations given the known perfect connections in these microstructures. However, the CI_1 metric yielded contrasting results, particularly for the first three examples (Fig. 6 a, b, and c), indicating a poor connection or one significantly distant from perfection. Despite the inherent perfect connection in these microstructures, the non-symmetric geometry about the interface rendered CI_1 an inadequate indicator of their connection quality. This observation underscores the limitation of CI_1 in capturing the intricacies of non-symmetric connections accurately.

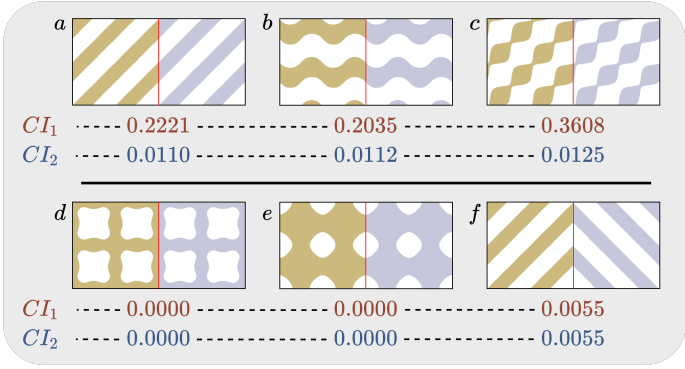

FIGURE 6: SIX PAIRS OF MICROSTRUCTURES, WITH THREE EXHIBITING SYMMETRY (D, E, AND F) ABOUT THEIR INTERFACE AND THREE ASYMMETRIES (A, B, AND C). SINCE THE SELECTION PROCESS WAS DELIBERATE, ALL PAIRS HAVE THE BEST CONNECTION POSSIBLE AT THEIR INTERFACES, SO THE CIS ARE EXPECTED TO BE SMALL AND CLOSE TO 0. THE CI_2 METRIC DEMONSTRATED ITS EFFECTIVENESS BY YIELDING VALUES CLOSE TO ZERO ($CI_2 \simeq 0$) IN ALL SIX CASES. THE CI_1 METRIC FOR THE FIRST THREE EXAMPLES (A, B, AND C), INDICATES A POOR CONNECTION AND WAS ABLE TO DETECT THE PERFECT CONNECTION FOR THE SYMMETRIC PAIRS (D, E, AND F).

Conversely, for the subsequent three samples (Fig. 6 d, e, and f), CI_2 performed admirably, signaling proper connections in all instances. This successful application underscores the robustness and reliability of CI_2 for assessing microstructural connections, particularly in scenarios with non-symmetric geometries. These results highlight the effectiveness of the CI_2 metric in quantifying microstructural connections across diverse scenarios. The limitations of CI_1, particularly in non-symmetric configurations, underscore the importance of employing metrics tailored to the specific characteristics and requirements of the microstructures under evaluation.

3.2 Integrating CI into Design Principles

Flexibility in selecting the most suitable κ value is enabled by integrating CI metric, allowing for informed decisions and effective optimization of microstructural designs. The subsequent analysis involved solving a minimum optimization problem with the κ as the optimization variable and CI_2 as the objective. Figure 7 plots the CI_2 versus the κ for a two-cell structure. The CI_2 is calculated at the interface of the two microstructures. It should be noted that a perfect connection $CI_2 = 0$ is hard to achieve, but numerical investigations shows that a $CI_2 \leq 0.05$ is a reasonably good connection.

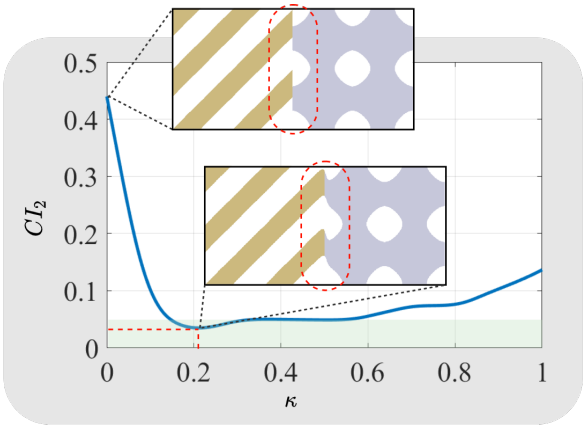

FIGURE 7: ILLUSTRATION OF CI_2 VERSUS THE κ FOR A TWO-CELL STRUCTURE. $\kappa = 0$ THE CONNECTION IS FLAWED, AND THE $CI_2 = 0.42$. THE MINIMUM VALUE OF $CI_2 = 0.2$ WAS ACHIEVED BY $\kappa = 0.21$. A PERFECT CONNECTION $CI_2 = 0$ IS HARD TO ACHIEVE, SO THE BLUE CURVE RARELY REACHES 0. BUT A $CI_2 \leq 0.05$ IS A REASONABLY GOOD CONNECTION, WHICH IMPLIES ANY κ RESULTING IN A CI_2 IN THE GREEN REGION IS ACCEPTABLE.

Figure 8 illustrates the connection between two microstructures. In the first row, the unit cells are depicted prior to the functional-gradation process (no κ value). The connection appears flawed, exhibiting poor connectivity with multiple points of discontinuity at the interface, potentially leading to stress concentration and inefficient load transfer. Let's assess if the Connectivity Index can detect this issue. CI_2 registers a value of 0.42, indicating a problematic connection. Similarly, CI_1 quantifies the poor connection, recording $CI_1 = 0.43$. We also applied the presented microstructure-embedding with three different κ values—0.15, 0.30, and 0.45—to the second, third, and fourth rows from the top, respectively (refer to Fig. 8). While visually the connection appears significantly improved for all three cases, each CI reveals a distinct and noteworthy narrative. The second row can be disregarded, as both CIs are large, indicating continued poor connection. In contrast, the third and fourth rows exhibit relatively small $CI_2 < \varepsilon$, suggesting a substantial improvement in connection for both cases. However, the CI_1 value for the fourth row is notably higher than that for the third row. Despite the larger CI_1 value, it should not be interpreted as indicating a poor connection, considering the CI_2 value and visual confirmation.

What might account for the high CI_1 metric? As previously explained, CI_1 is formulated to be highly sensitive to asymmetric connections. Thus, the slightly less symmetric configuration of

Copyright © 2025 by ASME

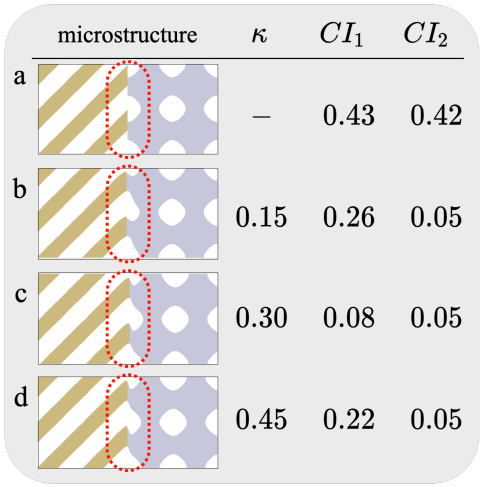

FIGURE 8: COMPARISON BETWEEN CI_1 AND CI_2 VALUES BEFORE AND AFTER APPLICATION OF THE WEIGHTED INTERPOLATION WITH THREE FIXED κ.

the microstructures in the fourth row (Fig. 8d) about the interface line, compared to those in the third row (Fig. 8c), has caused such discrepancies. In this case, different acceptable results ($CI_2 < \varepsilon$) were obtained for different κ values by CI_2. Although CI_1 was not found to work well on non-symmetric connections, it can be employed as a supplementary criterion to aid in the selection process.

The second pair of different microstructure connections is showcased in Fig. 9. Similar to the previous example, the connection before the functional gradation is depicted in the first row, where no κ is associated with this row. Although the left-side microstructure is fully connected to the right side, sharp transitions exist at the interface, resulting in $CI_2 = 0.30$ and $CI_1 = 0.58$. The subsequent three rows illustrate how the functional gradation transforms the sharp transition into a smooth and gradual one.

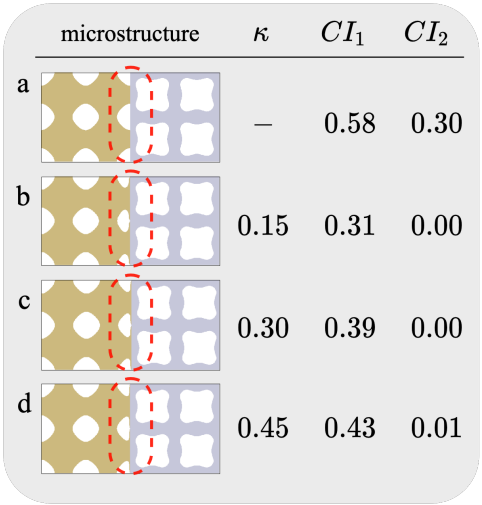

FIGURE 9: COMPARISON BETWEEN CI_1 AND CI_2 VALUES BEFORE AND AFTER APPLICATION OF THE WEIGHTED INTERPOLATION WITH THREE FIXED κ.

To determine the proper κ for this example, the analysis begins with CI_2. Since CI_2 is zero for rows two and three (Fig. 9b, and c), the selection prioritizes the one generating the smaller CI_1, which is $\kappa = 0.15$. Despite using CI_1 as a supplementary criterion, it does not significantly respond to changes at the interface. This underscores another limitation of the CI_1 metric, as it fails to discern improvements at the interface in cases where the structures lack symmetry about the interface line. Its dependency on symmetry disregards the transition from a sharp interface to a smooth one.

For the third pair (Fig. 10), two microstructures were deliberately chosen to exhibit symmetry about the interface in their transition region. The materials are connected, yet sharp points emerge due to the convergence of microstructures at the interface (see Fig. 10a). Through the application of functional gradation and assignment of different values to κ, these sharp points were eliminated, achieving a smooth connection. CI_2 successfully observed the improvements, dropping from 0.01 to an absolute 0.00. However, there are no indications of improvement in CI_1 values for the other rows. CI_1 remains equal to 0.01 for all four rows. It can be interpreted that according to CI_1, the connection in the third row (Fig. 10c) is no better than the connection in the first row (before gradation, Fig. 10a).

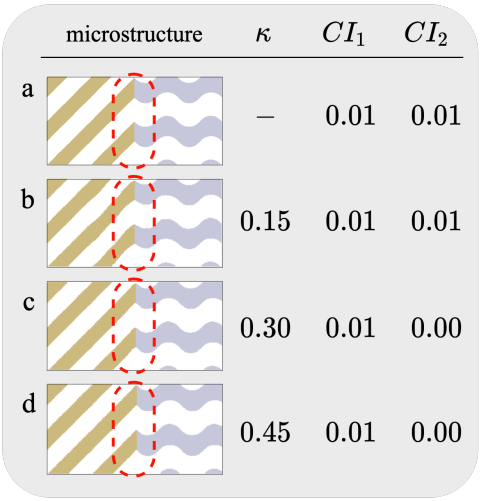

FIGURE 10: COMPARISON BETWEEN CI_1 AND CI_2 VALUES BEFORE AND AFTER APPLICATION OF THE WEIGHTED INTERPOLATION WITH THREE FIXED κ.

Although it is indicated by the results that the introduced metric CI_2 is capable of observing bad connections, sudden changes, sharp transformations, and high localized stress points, the CI_1 was not completely ignored. In the design process of the best weight function for the functional-gradation scheme, CI_2 was used as the primary criterion, and CI_1 was utilized as the secondary or supplementary criterion. By considering both metrics, the decision-making process can potentially be enhanced, and a more robust evaluation of microstructural designs can be ensured. This approach allows for flexibility and adaptability in selecting the most suitable κ value based on the specific requirements and constraints of the application. By integrating multiple metrics, the strengths of each can be leveraged to make more informed decisions and effectively optimize microstructural designs.

Copyright © 2025 by ASME

3.3 Application of CI in 3D Architected Materials

All the examples in the previous section were selected based on their clear representation, which is why they were all 2D materials. Now that the influence of the reliable metric (CI_2) on the process of functional gradation for microstructures has been established, In this section, we apply it to 3D architected materials.

For the first 3D microstructure connectivity study, three pairs of Diamond-Diamond, F_2-Diamond, and Gyroid-Primitive functionally represented microstructures were chosen (see Fig. 11). Again, let's begin with our expectations regarding their connectivity indices. For the first pair - Diamond-Diamond (Fig. 11a) - we expect the CI to be approximately 0. The Diamond structure has three planes of symmetry, so the interface of two identical Diamond microstructures should have no discontinuity or sharp changes. In other words, the right face of the left cell (Fig. 11a, the green area) is completely aligned with the left face of the right cell (Fig. 11a, the red area), indicating complete connection.

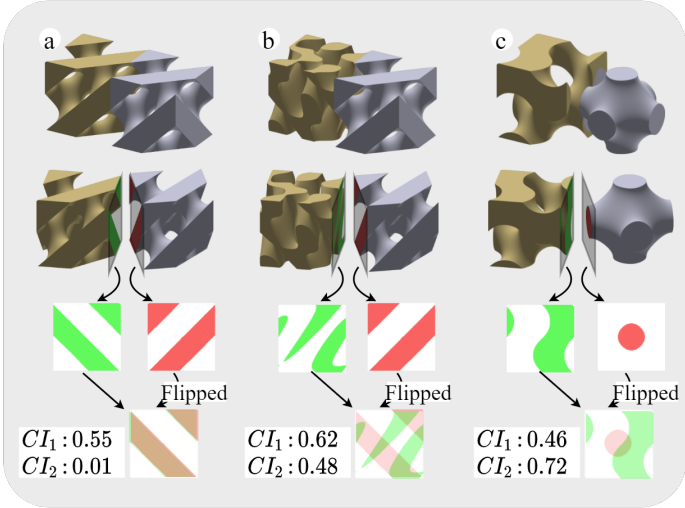

FIGURE 11: COMPARISON BETWEEN CI_1 AND CI_2 VALUES FOR THREE DELIBERATELY CHOSEN 3D STRUCTURES BEFORE APPLICATION OF THE WEIGHTED INTERPOLATION. A) WE EXPECT THE CI TO BE APPROXIMATELY 0. B) THE TOW CELLS HAVE PARTIAL CONNECTION. C) THE CELLS HAVE POOR CONNECTION SO WE EXPECT A LARGE CI VALUE, LARGER THAN THE OTHER TWO EXAMPLES.

For the next pair, Fig. 11b, the right face of the F_2 cell (Fig. 11b, the green area) and the left face of the Diamond cell (Fig. 11b, the red area) have partial overlap. For the last pair, Fig. 11c, the right face of the Gyroid cell (Fig. 11c, the green area) and the left face of the Primitive cell (Fig. 11c, the red area) have a very small overlap, which can be interpreted as the worst connection among the three pairs. So based on these, the expected CI values for the three pairs are $CI^a \simeq 0$, $CI^a < CI^b$, and $CI^b < CI^c$, where CI^a, CI^b, and CI^c are the CI values corresponding to pairs a, b, and c in Fig. 11, respectively. Between the CI_1 and CI_2 metrics, only CI_2 meets our expectations. The CI_2 values for the three pairs are $CI_2^a = 0.01$, $CI_2^b = 0.48$, and $CI_2^c = 0.72$, confirming the assumption ($CI \simeq 0$, and $CI^a < cI^b < CI^c$).

3.4 A Metric Beyond the Connectivity Index

Here, the possibility of extending the proposed metric to evaluate the integral robustness of the microstructures has been studied. Specifically, the metric has been evaluated at n different uniformly positioned points throughout the length of the microstructures see Fig. 12. The evaluation results are summarized in this section.

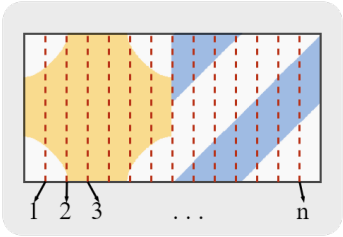

FIGURE 12: HYPOTHETICALLY DIVIDING THE STRUCTURE INTO n DIFFERENT UNIFORMLY POSITIONED SECTIONS THROUGHOUT THE LENGTH OF THE MICROSTRUCTURES, SO THE CI CAN BE CALCULATED AT EACH ONE OF THESE INTERFACES.

The CI_2 metric, by definition, serves as a quantification of the connection between entities positioned on its right and left sides. The intention is to utilize this metric to identify any discontinuities or localized stress points not only at the interface of microstructures but also within the microstructure itself. Figure 13 showcases 4 pairs of microstructures, where Pair-a and Pair-b visualize the cells before and after functional gradations respectively; pair c and pair d visualize different microstructures before and after the gradation. For all these four pairs, the CI_2 was calculated at 200 uniformly spaced points along the X-direction ($n = 200$).

In Fig 13a, particularly the CI_2 plot, it is noted that $0 \leq CI \leq 1$, and large CI_2 values indicate significant imperfections, as per its definition. It is observed that there is an imperfection at the middle of the pair ($CI_2 \simeq 0.5$), which is known to be caused by the poor connectivity of the two microstructures. Upon examining Fig. 13b, it is evident that after applying functional gradation (addressing the connectivity-issue), the jump in the CI_2 plot disappears.

In Fig 13c and the corresponding CI_2 plot, three imperfections are identified in this pair. The first imperfection (at the middle of the pair) is attributed to the poor connectivity of the two microstructures. However, the second and third imperfections result from sudden changes within the microstructure, which are part of its design and do not pertain to connectivity issues. Depending on the application of the designed structure, the second and third jumps in CI_2 might not be negligible. Identifying these imperfections at x_2 and x_3, smooth gradation can be applied to address them inside the microstructure. As they do not pertain to connectivity issues, they are disregarded at present, with plans to address these types of imperfections in future studies. Nonetheless, the first jump in CI_2 is mitigated by applying functional gradation at the interface of the two unit cells. Figure 13c illustrates how functional gradation diminishes the first jump, leaving no trace of it in Fig. 13d.

Copyright © 2025 by ASME

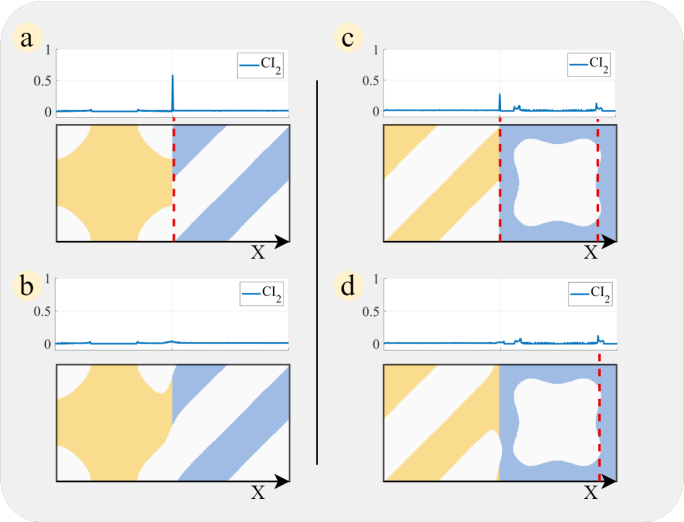

FIGURE 13: CALCULATE THE CI_2 AT n HYPOTHETICAL INTERFACE THROUGHOUT THE STRUCTURE, ALL PERPENDICULAR TO THE X AXIS. A) ONLY ONE IMPERFECTION DETECTED ($CI_2 > 0.05$). B) THE IMPERFECTION DISSOLVED AFTER APPLYING THE WEIGHTED INTERPOLATION AT THE INTERFACE (NO $CI_2 > 0.05$). C) TWO IMPERFECTIONS ARE DETECTED. D) ONLY ONE WAS RESOLVED BY APPLICATION OF WEIGHTED INTERPOLATION.

4. DISCUSSION AND CONCLUSION

This study has presented a novel approach to enhance connectivity in microstructures, addressing critical challenges in multi-scale design optimization. By introducing a novel connectivity index (CI), we have addressed the limitations of prior methods, enabling the identification and rectification of imperfections at the micro-scale level. The connectivity index is particularly beneficial due to its ability to detect flaws in connectivity at the micro-level that might lead to stress concentration and inefficient load transfer. Utilizing the introduced CI not only ensures proper connectivity between microstructural elements but also facilitates the detection of irregularities within microstructures, enhancing the reliability and performance of architected materials. We presented a weight selection approach for a functional gradation at the micro-level based on the CI value. This approach offers flexibility in selecting the most suitable κ value based on specific application requirements and constraints. By integrating a well-defined CI metric, informed decisions can be made to optimize microstructural designs effectively. This integration ensures smoother transitions and enhances robustness by optimizing connectivity between microstructures.

In summary, the recognition of poor connections through the CI metric underscores the need for continuous refinement and optimization in microstructural design processes. By leveraging multiple metrics and addressing identified issues, designers can strive towards achieving microstructures that exhibit improved connectivity and better overall performance. The results presented in the previous section underscore the versatility and applicability of the CI_2 metric beyond its conventional usage at the interface of microstructures. The connectivity index can be more than a quantifying metric, it can be used to find imperfections in the structures. By extending its evaluation to multiple points within the microstructure, the CI_2 metric can effectively identify imperfections, discontinuities, and localized stress points throughout the structure. When the connectivity index suggests a poor connection, it highlights potential areas for improvement or adjustment in the microstructural design. This capability enables designers and engineers to pinpoint regions of the problem and put into effect targeted interventions to enhance the overall integrity and performance of the microstructure. By strategically applying gradation at critical points, designers can achieve smoother transitions, mitigate stress concentrations, and optimize the structural performance of the material.

We showed that there are cases where CI_2 yields multiple acceptable results for different κ values, its integration with CI_1 proves beneficial. Although we mentioned that CI_1 may not perform well in detecting improvements in non-symmetric connections, it can serve as a supplementary criterion to aid in the selection process. The discrepancies between previously introduced connectivity index (CI_1) and our new connectivity index (CI_2) emphasize the complexity of evaluating microstructural designs and the necessity of employing comprehensive methodologies. We showed that integrating both metrics allows for a more thorough assessment and facilitates more informed decision-making processes. By considering both metrics, the decision-making process is enhanced, leading to a more robust evaluation of microstructural designs.

Overall, the integration of both the CI_1 and CI_2 metrics, provides a comprehensive approach to microstructure design and optimization. By leveraging these tools, designers can create robust and efficient microstructures tailored to specific applications and performance requirements, ultimately advancing the field of materials science and engineering. In our forthcoming research, we aim to thoroughly investigate the full potential for discovering and identifying imperfections within microstructures using the CI, extending beyond the scope of interface analysis. We will delve into available methodologies to effectively detect and address these imperfections within an optimization design framework.

ACKNOWLEDGMENT

We acknowledge the support from the National Science Foundation (NSF) through CMMI-2245298.

REFERENCES

[1] Corni, I, Harvey, TJ, Wharton, JA, Stokes, KR, Walsh, FC and Wood, RJK. "A review of experimental techniques to produce a nacre-like structure." *Bioinspiration & biomimetics* Vol. 7 No. 3 (2012): p. 031001.

[2] Tan, Ting, Rahbar, N, Allameh, SM, Kwofie, S, Dissmore, D, Ghavami, K and Soboyejo, WO. "Mechanical properties of functionally graded hierarchical bamboo structures." *Acta biomaterialia* Vol. 7 No. 10 (2011): pp. 3796–3803.

[3] Fernandes, Matheus C, Aizenberg, Joanna, Weaver, James C and Bertoldi, Katia. "Mechanically robust lattices inspired by deep-sea glass sponges." *Nature Materials* Vol. 20 No. 2 (2021): pp. 237–241.

[4] Senhora, Fernando V, Sanders, Emily D and Paulino, Glaucio H. "Optimally-Tailored Spinodal Architected Materials

Copyright © 2025 by ASME

for Multiscale Design and Manufacturing." *Advanced Materials* Vol. 34 No. 26 (2022): p. 2109304.

[5] Pawlyn, Michael. *Biomimicry in architecture*. Routledge (2019).

[6] Shalaev, Vladimir M. "Optical negative-index metamaterials." *Nature photonics* Vol. 1 No. 1 (2007): pp. 41–48.

[7] Grima, Joseph N and Evans, Kenneth E. "Auxetic behavior from rotating squares." *Journal of materials science letters* Vol. 19 (2000): pp. 1563–1565.

[8] Chen, Tian, Panetta, Julian, Schnaubelt, Max and Pauly, Mark. "Bistable auxetic surface structures." *ACM Transactions on Graphics (TOG)* Vol. 40 No. 4 (2021): pp. 1–9.

[9] Takezawa, Akihiro, Kobashi, Makoto and Kitamura, Mitsuru. "Porous composite with negative thermal expansion obtained by photopolymer additive manufacturing." *APL Materials* Vol. 3 No. 7 (2015).

[10] Berger, JB, Wadley, HNG and McMeeking, RM. "Mechanical metamaterials at the theoretical limit of isotropic elastic stiffness." *Nature* Vol. 543 No. 7646 (2017): pp. 533–537.

[11] Fujii, D, Chen, BC and Kikuchi, Noboru. "Composite material design of two-dimensional structures using the homogenization design method." *International Journal for Numerical Methods in Engineering* Vol. 50 No. 9 (2001): pp. 2031–2051.

[12] Rodrigues, Hélder, Guedes, Jose M and Bendsoe, MP. "Hierarchical optimization of material and structure." *Structural and Multidisciplinary Optimization* Vol. 24 (2002): pp. 1–10.

[13] Liu, Ling, Yan, Jun and Cheng, Gengdong. "Optimum structure with homogeneous optimum truss-like material." *Computers & Structures* Vol. 86 No. 13-14 (2008): pp. 1417–1425.

[14] Zhu, Bo, Skouras, Mélina, Chen, Desai and Matusik, Wojciech. "Two-scale topology optimization with microstructures." *ACM Transactions on Graphics (TOG)* Vol. 36 No. 4 (2017): p. 1.

[15] Chen, Wenjiong, Tong, Liyong and Liu, Shutian. "Concurrent topology design of structure and material using a two-scale topology optimization." *Computers & Structures* Vol. 178 (2017): pp. 119–128.

[16] Sanders, ED, Pereira, A and Paulino, GH. "Optimal and continuous multilattice embedding." *Science Advances* Vol. 7 No. 16 (2021): p. eabf4838.

[17] Bensoussan, Alain, Lions, Jacques-Louis and Papanicolaou, George. *Asymptotic analysis for periodic structures*. Vol. 374. American Mathematical Soc. (2011).

[18] Bendsøe, Martin Philip and Kikuchi, Noboru. "Generating optimal topologies in structural design using a homogenization method." *Computer methods in applied mechanics and engineering* Vol. 71 No. 2 (1988): pp. 197–224.

[19] Sivapuram, Raghavendra, Dunning, Peter D and Kim, H Alicia. "Simultaneous material and structural optimization by multiscale topology optimization." *Structural and multidisciplinary optimization* Vol. 54 (2016): pp. 1267–1281.

[20] Coelho, Pedro G, Fernandes, Paulo R, Guedes, Jose M and Rodrigues, Hélder C. "A hierarchical model for concurrent material and topology optimisation of three-dimensional structures." *Structural and Multidisciplinary Optimization* Vol. 35 (2008): pp. 107–115.

[21] Du, Zongliang, Zhou, Xiao-Yi, Picelli, Renato and Kim, H Alicia. "Connecting microstructures for multiscale topology optimization with connectivity index constraints." *Journal of Mechanical Design* Vol. 140 No. 11 (2018): p. 111417.

[22] Alexandersen, Joe and Lazarov, Boyan S. "Topology optimisation of manufacturable microstructural details without length scale separation using a spectral coarse basis preconditioner." *Computer Methods in Applied Mechanics and Engineering* Vol. 290 (2015): pp. 156–182.

[23] Xie, Yi Min, Zuo, Zhi Hao, Huang, Xiaodong and Rong, Jian Hua. "Convergence of topological patterns of optimal periodic structures under multiple scales." *Structural and Multidisciplinary Optimization* Vol. 46 (2012): pp. 41–50.

[24] Coelho, PG, Amiano, LD, Guedes, JM and Rodrigues, HC. "Scale-size effects analysis of optimal periodic material microstructures designed by the inverse homogenization method." *Computers & Structures* Vol. 174 (2016): pp. 21–32.

[25] DUMONTET, Hélène. "Boundary layers stresses in elastic composites." *Studies in Applied Mechanics*. Vol. 12. Elsevier (1985): pp. 215–232.

[26] Schumacher, Christian, Bickel, Bernd, Rys, Jan, Marschner, Steve, Daraio, Chiara and Gross, Markus. "Microstructures to control elasticity in 3D printing." *ACM Transactions on Graphics (Tog)* Vol. 34 No. 4 (2015): pp. 1–13.

[27] Zhou, Shiwei and Li, Qing. "Design of graded two-phase microstructures for tailored elasticity gradients." *Journal of Materials Science* Vol. 43 (2008): pp. 5157–5167.

[28] Radman, Arash, Huang, Xiaodong and Xie, YM. "Topology optimization of functionally graded cellular materials." *Journal of Materials Science* Vol. 48 (2013): pp. 1503–1510.

[29] Deng, Jiadong and Chen, Wei. "Concurrent topology optimization of multiscale structures with multiple porous materials under random field loading uncertainty." *Structural and Multidisciplinary Optimization* Vol. 56 (2017): pp. 1–19.

[30] Wang, Yiqiang, Chen, Feifei and Wang, Michael Yu. "Concurrent design with connectable graded microstructures." *Computer Methods in Applied Mechanics and Engineering* Vol. 317 (2017): pp. 84–101.

[31] Rastegarzadeh, Sina, Wang, Jun and Huang, Jida. "Implicitly Represented Architected Materials for Multi-Scale Design and High-Resolution Additive Manufacturing." *Advanced Materials Technologies* Vol. 8 No. 17 (2023): p. 2300274.

[32] Rastegarzadeh, Sina, Wang, Jun and Huang, Jida. "Multiscale topology optimization with neural network-assisted optimizer." *International Design Engineering Technical Conferences and Computers and Information in Engineer-*

Copyright © 2025 by ASME

ing Conference, Vol. 86212: p. V002T02A041. 2022. American Society of Mechanical Engineers.

[33] Rastegarzadeh, Sina, Wang, Jun and Huang, Jida. "Neural Network-Assisted Design: A Study of Multiscale Topology Optimization With Smoothly Graded Cellular Structures." *Journal of Mechanical Design* Vol. 145 No. 1 (2023): p. 011701.

[34] Von Schnering, HG and Nesper, R. "Nodal surfaces of Fourier series: fundamental invariants of structured matter." *Zeitschrift für Physik B Condensed Matter* Vol. 83 No. 3 (1991): pp. 407–412.

[35] Wang, Jun and Huang, Jida. "Functionally Graded Non-Periodic Cellular Structure Design and Optimization." *Journal of Computing and Information Science in Engineering* (2021): pp. 1–10.

[36] Rastegarzadeh, Sina, Wang, Jun and Huang, Jida. "Two-Scale Topology Optimization With Parameterized Cellular Structures." *International Design Engineering Technical Conferences and Computers and Information in Engineering Conference*, Vol. 85376: p. V002T02A046. 2021. American Society of Mechanical Engineers.

Copyright © 2025 by ASME